International Journal of Concrete Structures and Materials

RESEARCH

Open Access

Structural Behavior of Ultra-High Strength Concrete Columns Reinforced with Basalt Bars Under Axial Loading

Taha A. El-Sayed[1*], Kareem S. Abdallah[1], Hossam E. Ahmed[1] and Tamer H. El-Afandy[2]

Abstract

The axial compressive behavior of Ultra-High Strength Concrete (UHPC) columns reinforced with basalt bars was investigated in this work. Only a few research projects have used basalt Reinforced Concrete Columns. Under axial stress, 12 columns of 150 × 150 mm in cross section and 1200 mm in height manufactured of M120 grade UHPC, incorporating glass powder lime powder, were tested. The primary characteristics investigated in this study were axial load capacity, axial deformation, failure pattern, ductility, and stiffness. The findings of the experimental tests revealed that the ultimate loads and behavior of UHPCC reinforced with BFRP were superior to concrete columns strengthened with steel reinforcement. When compared to steel RC columns, basalt RC columns carry about 90% of the axial load. Moreover, the BFRP bar tensile strength was 2.5 greater than reinforcing steel yield strength and 1.79 times larger than that of bar. The Ansys software-based analytical analysis assisted in predicting the eventual carrying capacity of UHPC columns. The agreement among the experimental and NLFE ultimate load is around 92.2%, with a standard deviation of 0.005 and a coefficient of variation of 0.00002. The nonlinear BFRP–UHPC columns' structural performance was adequately predicted by the finite element analysis. In addition, equations are employed to forecast the strength of confined concrete. Equation 4 merely produced improved forecasts, it aids in comparing the outcomes of analytical and experimental tests. Results of this study indicated that the UHPC-columns reinforced with BFRP bars offer potential economic and environmental advantages as compared to traditional RC columns.

Keywords UHPC-columns, Basalt-bars, Compressive behavior, Non-linear study, Ansys

1 Introduction

In recent decades, corrosion in harsh environmental conditions has mostly harmed RC constructions. It is causing a decrease in strength and efficiency. Several researches have been carried out to boost concrete strength and tackle corrosion issues. High-strength concrete is being marketed for usage in a wide range of building applications. HSC provides greater advantages than regular-strength concrete. Its HSC is more robust, and the designer decreases the element's cross-sectional area. On the industrial side, they are creating high-strength concrete using non-corroding GFRP bars as alternative reinforcement. Reinforcement concrete constructions finished HSC with GFRP bars, extending the structural parts' service life. To accommodate the world highly evolved human civilizations, more and higher effective designs are required nowadays (Adam et al., 2021; El-Sayed et al., 2022; Erfan et al., 2020; Nassif et al., 2021; Yu et al., 2021, 2022).

UHPFRC is a potential construction material with excellent self-consolidating properties, high durability resistance, and high mechanical strength, making it appealing for high-performance foundation designs.

Journal information: ISSN 1976-0485 / eISSN 2234-1315

*Correspondence:
Taha A. El-Sayed
taha.ibrahim@feng.bu.edu.eg
[1] Department of Structural Engineering, Shoubra Faculty of Engineering, Benha University, Cairo, Egypt
[2] Housing and Building National Research Centre, Giza, Egypt

Currently, the majority of research is focused on exploring UHPFRC mix improvements (Xie et al., 2018a; Yoo et al., 2015), UHPFRC beams, columns and slabs flexural performance (Abadel et al., 2022a, 2023; Baby et al., 2013, 2014; El-Sayed, 2021; El-Sayed & Algash, 2021; Lachance et al., 2016; Mahmud et al., 2013), and UHPFRC elements reaction under blast pressures (Millard et al., 2010). Because of developments in concrete technology, high-performance concrete is now accessible and employed HPC. Concerns have been raised concerning the efficiency of HPC columns, as the use of HPC to reduce cross-sectional dimensions favors the building of RC columns over conventional strength concrete (Hung & Hu, 2018).

Shin et al. (Shin et al., 2015, 2017, 2018) and Hosinieh et al. (Hosinieh et al., 2015) discovered that lowering the distance between the transverse reinforcements of the short column considerably boosted the force bearing capacities and force sustainability after peak in their research of the pure axial behaviors of short columns. Adding extra crossties for transverse reinforcements with predetermined stirrup spacing would just raise the overall toughness of the short columns without considerably boosting their force bearing capacities. Steel fibers were present at the time, which kept the concrete from spalling during failure and boosted the post-peak ductility of the columns (Fang et al., 2019).

Palacios et al. (Palacios, 2015) also studied the cyclic efficiency of a column with a UHPC-fabricated plastic hinge region. The results of their research showed that using UHPC changed the typical mechanism of failure of RC columns with confinement increase and prevented concrete crushing. Several experimental and computational studies have been conducted in recent decades to examine the achievement of structures reinforced by FRP bars due to steel reinforcement corrosion, which is one of the major problems that shortens the lifetime serviceability and, thus, brittle failure of many concrete structures worldwide. FRP materials have recently become a viable material for manufacturing reinforcement bars for concrete buildings (American Concrete Institute (ACI) 2006).

Afifi et al. (Afifi et al., 2014a) studied the efficacy of circular columns reinforced with CFRP bars and spirals. He discovered that the CFRP bars were successful in sustaining compression until the concrete was crushed and provided an average of 12% of column capacity. Mohamed (Mohamed et al., 2014), also examined 14 full-scale circular RC columns under concentric axial stress with longitudinal Sand-coated GFRP bars and carbon-FRP (CFRP) restricted with circular hoops or FRP spirals. He stated that it offered enough restriction against buckling of the longitudinal FRP bars and satisfactory confinement of the concrete core in the post peak periods. Flexural and stress behavior of FRP-RC parts has recently been thoroughly studied (Canada, 2009).

However, it was still unknown how FRP-RC columns would behave under axial compression. However, FRP bars are not advised for use as longitudinal reinforcement in columns according to ACI 440.1R-06 (American Concrete Institute (ACI) 2006). Further study in this area is called for by ACI 440.1R-06 (American Concrete Institute (ACI) 2006), while Canadian standards (Canadian Standards Association, 2012) ignore the importance of FRP longitudinal reinforcement's compressive resistance in the compression zone in compressive and flexural concrete components. Previous studies have shown that FRP bars have lower strength and modulus in compression than in tension (Chaallal & Benmokrane, 1993; Wu, 1990).

CFRP bars have been found to have a compressive strength that is 78% of their tensile strength (Mallick, 1988; Wu, 1990). In addition, recent research on the bond behavior of conventional FRP rebars discovered that due to the distinctive characteristics of each FRP material and the variety of fiber/resin interfaces, it was difficult to anticipate bond behavior without doing experimental research.

In RC structures, BFRPs have gained popularity as an alternative to traditional FRPs (Refai et al., 2015). Ibrahim et al. (Ibrahim et al., 2015) used pull-out experiments to examine the bond-slip behavior among concrete and BFRP bars. He gave his OK for the reference to the well-known bond-slip presentation. BFRP is a potential substitute for other FRPs because of its lower cost, endurance to high temperatures, ease of production, and improved resistance to sulphate attack, chloride, effect stacking, and vibration (Lee et al., 2014; Li & Xu, 2009; Liu et al., 2015; Shi et al., 2011; Wei et al., 2010). BFRP bars may be incorporated into buildings in a number of different ways. A number of studies to assess the effectiveness of BFRP geopolymer concrete supporting components such columns, forbearing, and boards (Erfan et al., 2019a).

However, to effectively offer UHPC to as large a market as possible, its use must be envisioned as a catalyst for realizing innovative structural concepts, as opposed

Table 1 Basalt bars properties (ASTM, 2021; Erfan et al., 2019b)

Property	Measured value
Specific gravity (t/m^3)	2.68
Tensile strength (MPa)	1400
Tensile modulus (GPa)	56
Tensile strain (%ϵ_u)	25

Table 2 Mix design

Item	Cement (kg/m^3)	Fine aggregate (kg/m^3)	Silica Fume (kg/m^3)	Quartz Powder (kg/m^3)	Lime Powder (kg/m^3)	Superplasticizer (kg/m^3)	Water-binder –
Per m^3 of concrete	720	1105	220	170	180	55	0.18

Fig. 1 Typical concrete slump flow test for UHPSSC mix

Table 3 Specimen's description

Groups	Column ID	RFT. Type	Long. RFT	Trans. RFT
Group A	C1-A	Steel	4φ10	φ6@100
	C2-A	Steel	4φ10	φ6@150
	C3-A	Steel	4φ10	φ8@100
	C4-A	Steel	4φ10	φ8@150
Group B	C1-B	Steel	4φ12	φ6@100
	C2-B	Steel	4φ12	φ6@150
	C3-B	Steel	4φ12	φ8@100
	C4-B	Steel	4φ12	φ8@150
Group C	C1-C	Basalt	4φ12	φ6@100
	C2-C	Basalt	4φ12	φ6@150
	C3-C	Basalt	4φ12	φ8@100
	C4-C	Basalt	4φ12	φ8@150

to only being limited to incrementally improving current structural concepts and element thickness reduction. In addition, this complements specialist construction techniques, such as prefabrication and additive production, the use of which is otherwise unattainable (Abadel et al., 2022b; Abdellatief et al., 2023; Al-Obaidi et al., 2022; Ozbakkaloglu et al., 2018; Shang et al., 2022; Wang et al., 2022; Xie et al., 2018b; Zhu et al., 2022).

The main importance of this study is to examine the performance of using BFRP as longitudinal bars in the production of UHPSCC columns under axial stress, with varying stirrup diameters, spacing's, and steel reinforcement rebars. To achieve this goal, an experimental plan was carried out on twelve UHPC column specimens with dimensions 150 mm × 150 mm and height 1,200 mm that were subjected to axial loading. In addition, ANSYS® finite element code was used to create finite element models for all specimens to simulate structural behavior

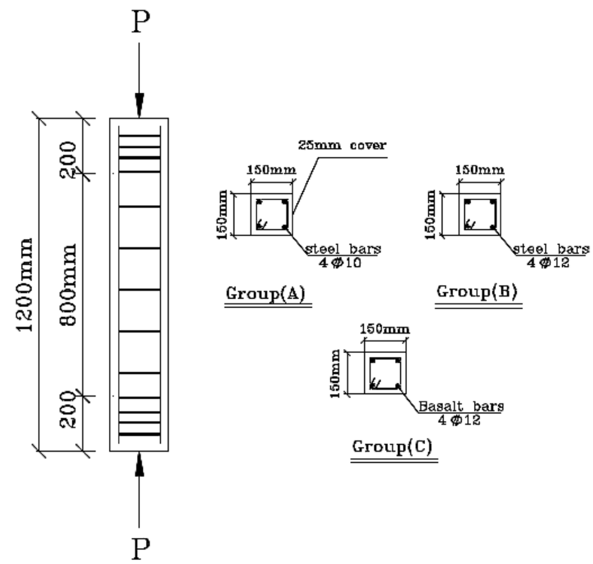

Fig. 2 Columns typical dimensions and internal reinforcement details

Fig. 3 Test setup

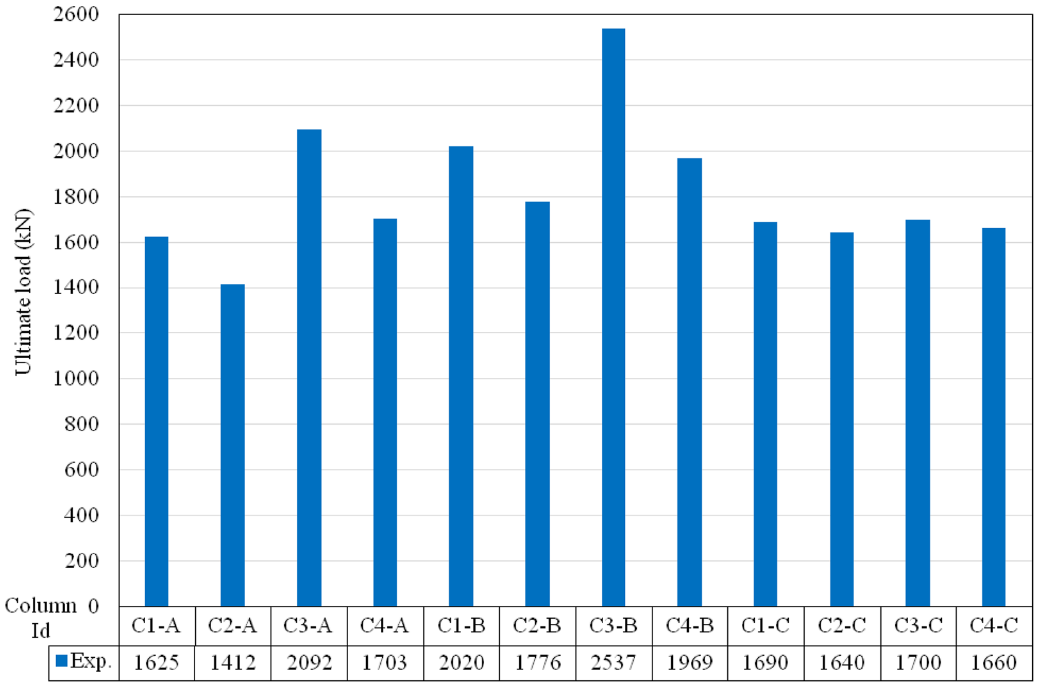

Fig. 4 Ultimate load of tested columns

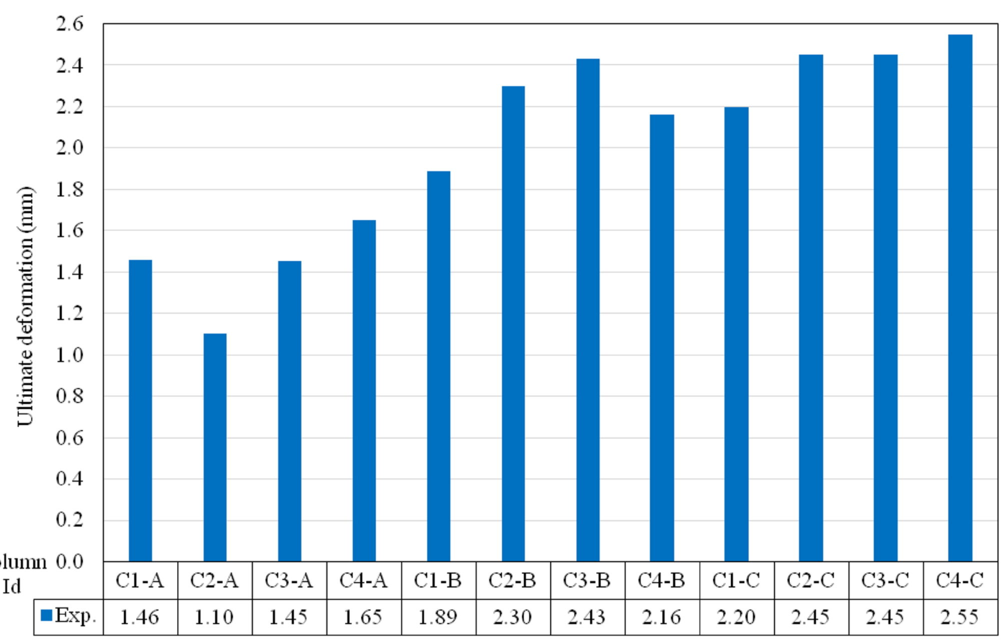

Fig. 5 Ultimate deflection of tested columns

of each specimen. Based on such investigations, additional stiffeners and UHPC were used to increase the load capacity of columns. When compared to RC columns, test findings show that basalt bars contributed about 90% of the outcomes.

1.1 Significance of Research

Eight steel-reinforced and four basalt-reinforced RC columns that had been exposed to axial stresses each were used in the current study. The findings of the experimental investigation are contrasted with those of the

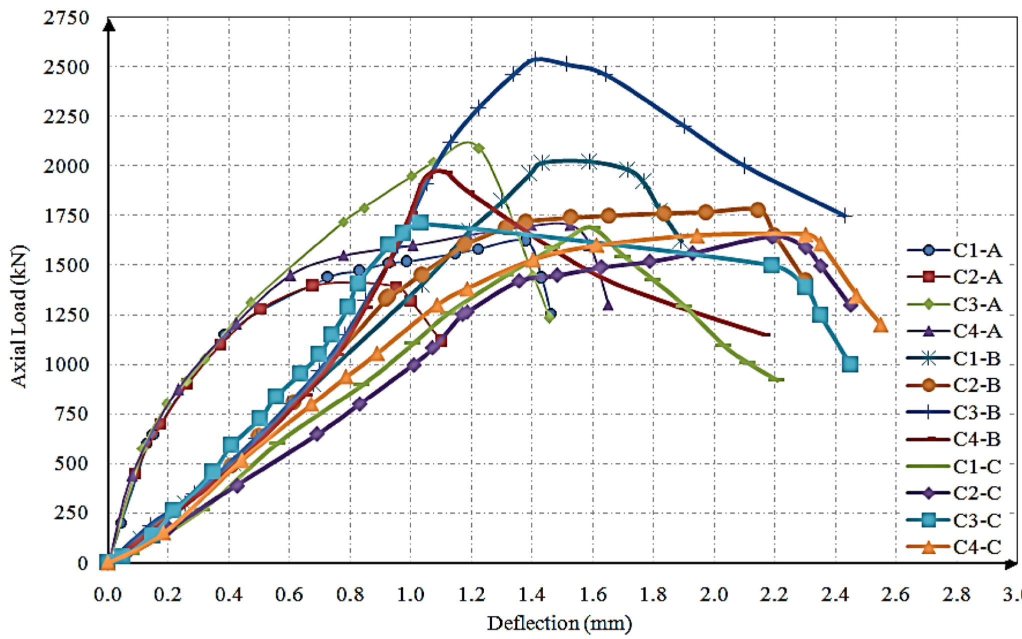

Fig. 6 Load–deflection curves for all tested groups

analytical study. The detailed investigation would be as described in the following:

1. Analyzing the structural features of basalt-barred columns to ascertain their mechanism of failure
2. Assessing the basalt bars' compressive impact on concrete columns.
3. The non-linear Finite Element Model is examined by UHPC columns (FEM).
4. Analytical results are contrasted with experimental results. The outcomes of the analysis aid in predicting the axial stress on the column.

2 Experimental Study

2.1 Materials

1. Cement:

In this study, OPC-CEM I (52.5 N), compliant with EN 197/1 (EN, 2011), is employed. The silica fume used complies with ASTM (C1240-03a) and IS (15388-2003).

2. Aggregates

The specific density of natural quartz sand that meets ASTM (C33) standards is 2.60.

3. Lime powder

The specific gravity of lime powder (Ghareeb et al., 2022), a cement alternative substance, was 2.7.

4. Superplasticizer

The super plasticizer has a density of 1085 kg/m^3.

5. Steel bars:
   - Type I: 24/35, 8 mm diameter.
   - Type II: 42/60, 12 mm diameter.
6. Basalt bars:

12 mm diameter deformed basalt bars made locally. The characteristics of basalt bars are shown in Table 1.

2.2 Mix Design

The typical compressive strength of the design combination was estimated to be 120 MPa. Table 2 lists the properties of the mixture, while Fig. 1 display the flow of slump for this mix's self-compacted concrete column mixtures.

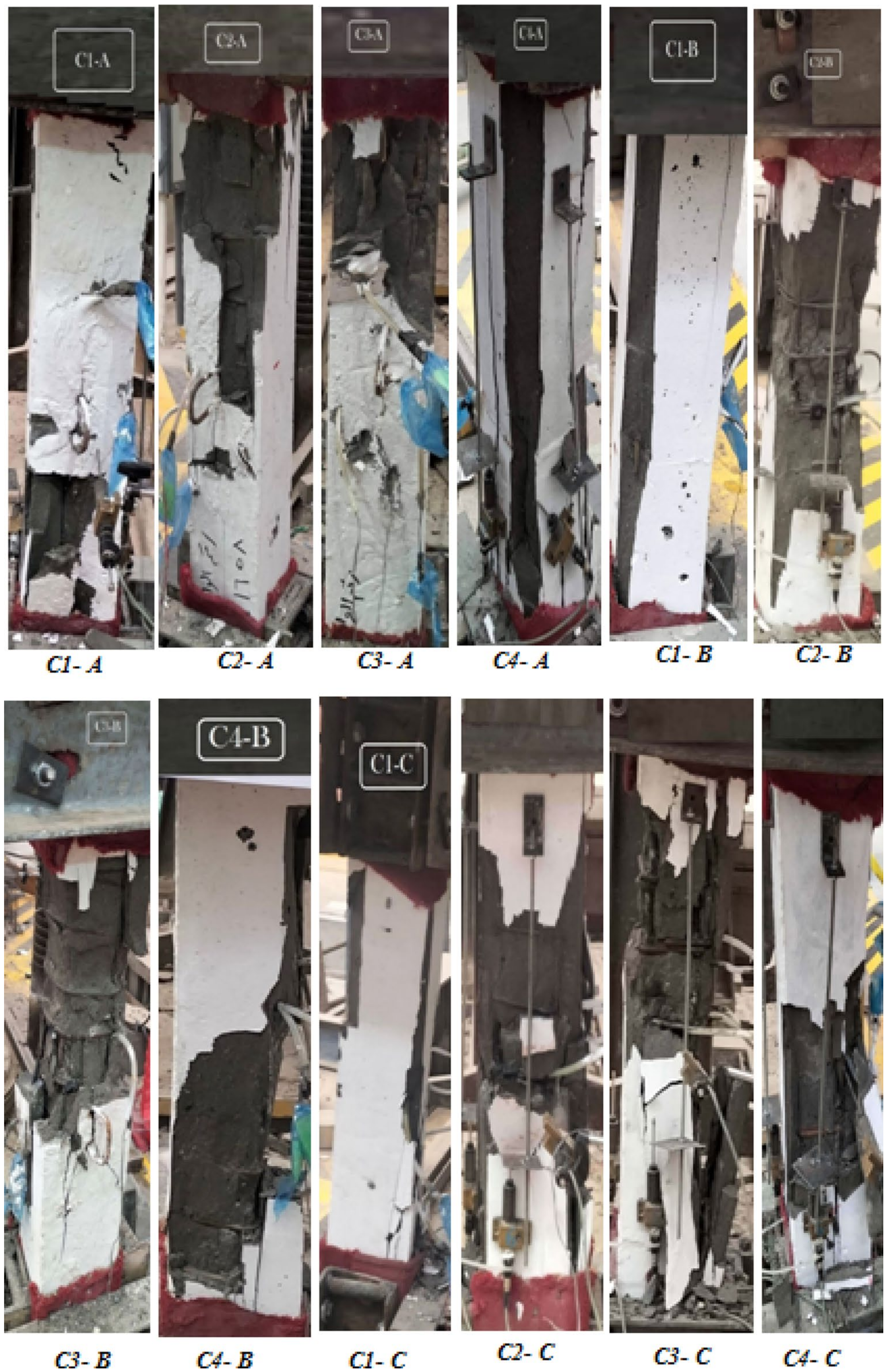

Fig. 7 Crack patterns for all column tested specimens

Table 4 Test results

Column ID	Ultimate load (kN)	Def. at Ult. load (mm)
C1-A	1625	1.46
C2-A	1412	1.10
C3-A	2092	1.45
C4-A	1703	1.65
C1-B	2020	1.89
C2-B	1776	2.30
C3-B	2537	2.43
C4-B	1969	2.16
C1-C	1690	2.20
C2-C	1640	2.45
C3-C	1700	2.45
C4-C	1660	2.55

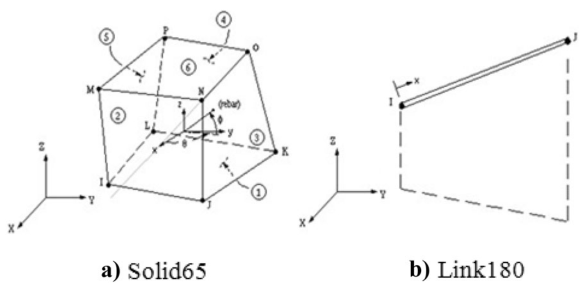

Fig. 8 Element type's geometry (ANSYS, 2005)

2.3 Experimental Program and Methodology

Table 3 and Fig. 2 present the information in 12 columns that used to examine the UHPSCC columns' overall behavior, cracking pattern, and final maximum capacity. The performance of concrete columns restrained by different numbers of stirrups and reinforced with either steel or BFRP reinforcements is assessed and analyzed. Table 3 presents the test matrix adopted in this study. All UHPSCC columns had a square cross section with dimensions of 150 mm × 150 mm, and a height of 1200 mm. The actual compressive strength was determined based on the average test results of nine concrete cubes (100 mm × 100 mm) tested on the same day as the start of testing of the column specimens. Two internal reinforcement schemes were employed.

2.4 Test Setup

All columns were examined using testing equipment with a capacity of 5000 kN. Fig. 3 depicts the column test configuration. The deformations of all the examined columns were monitored using an L.V.D.T. instrument till failure.

2.5 Test Results

2.5.1 Ultimate Load and Deformation

In this section, behavior of the tested column specimens in terms of ultimate load and deflection, the relationship between load and deflection, and cracking patterns are presented (see Figs. 4, 5, 6, 7). In addition, Table 4 provides a summary of experimental results.

2.5.2 Cracking Pattern

The cracking patterns of each column specimen are shown in Fig. 7.

3 Analytical Study

To assess the performance of the UHPC columns, a finite nonlinear analysis was conducted. Ansys was used to create FEM (ANSYS, 2005). FEM contributes in the prediction of the specimens' ultimate axial compressive load and failure.

3.1 Elements Type

Solid 65 was used to illustrate the stress–strain curve for concrete. While element Link 180 represented the bars and stirrups. Fig. 8 depicts the geometry of the element type.

3.2 Geometry Modeling

Columns are represented in the same manner as in the experimental test.

3.3 Modeling of Specimens

A finite nonlinear analysis was performed to evaluate the effectiveness of the UHPC columns represented in Fig. 9.

3.4 FEM the Constitutive Model

SOLID 65 was employed in the ANSYS software to simulate concrete elements, whereas Link 180 was employed to represent steel and BFRP bar elements. The curves used are shown in Fig. 10.

3.5 Materials Properties

The material characteristics for concrete and rebars reinforcement are shown in this section:

- **Concrete**

1. $E_c = 46{,}147.59$ MPa.
2. $\nu = 0.3$ (Ibrahim et al., 2015).

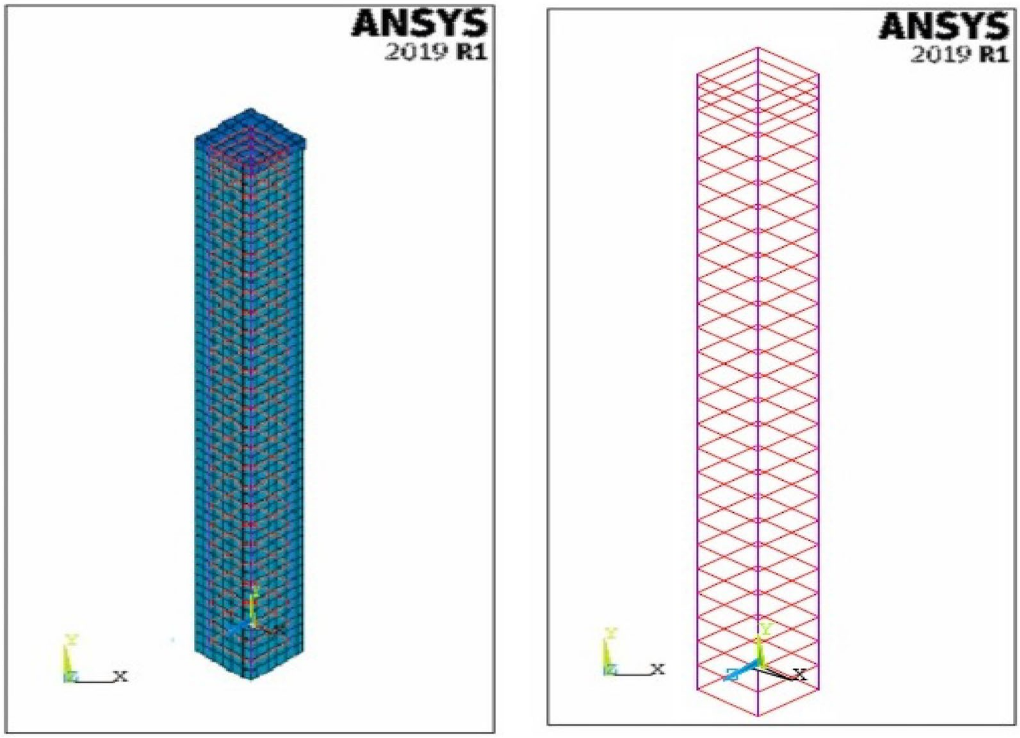

Fig. 9 Modeling of columns

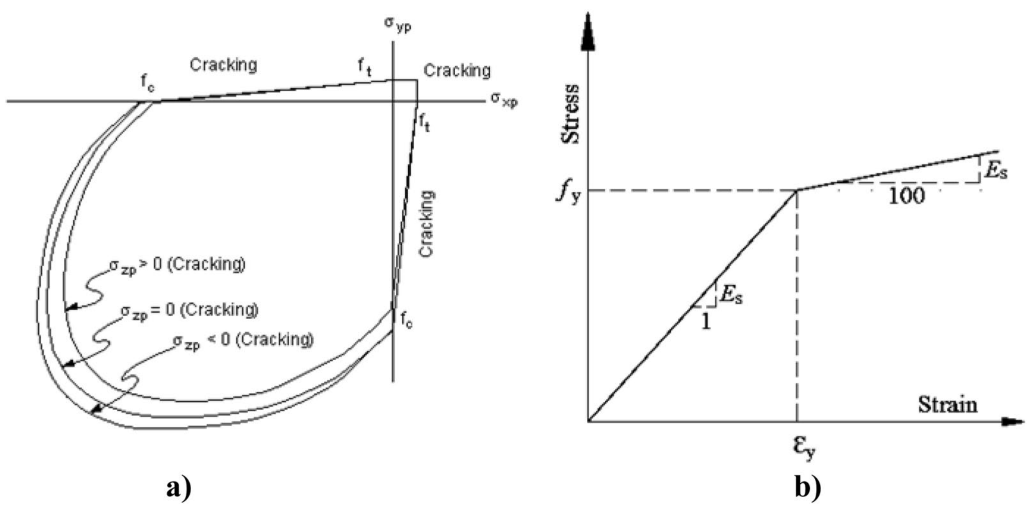

Fig. 10 Material behaviors; **a** solid 65- failure surface in principal stress space with nearly biaxial stress; **b** link180—bilinear stress–strain idealization

- **Steel rebars**

3. $E_s = 200$ kN/mm^2 (Ibrahim et al., 2015).
4. $f_y = 420$ MPa and $f_{yst} = 240$ MPa.
5. $\nu = 0.2$ (Ibrahim et al., 2015).
6. ϕ10 (As = 78.5 mm^2)
7. ϕ12 (As = 112 mm^2)
8. ϕ8 (As = 50.3 mm^2)
9. ϕ6 (As = 28.3 mm^2)

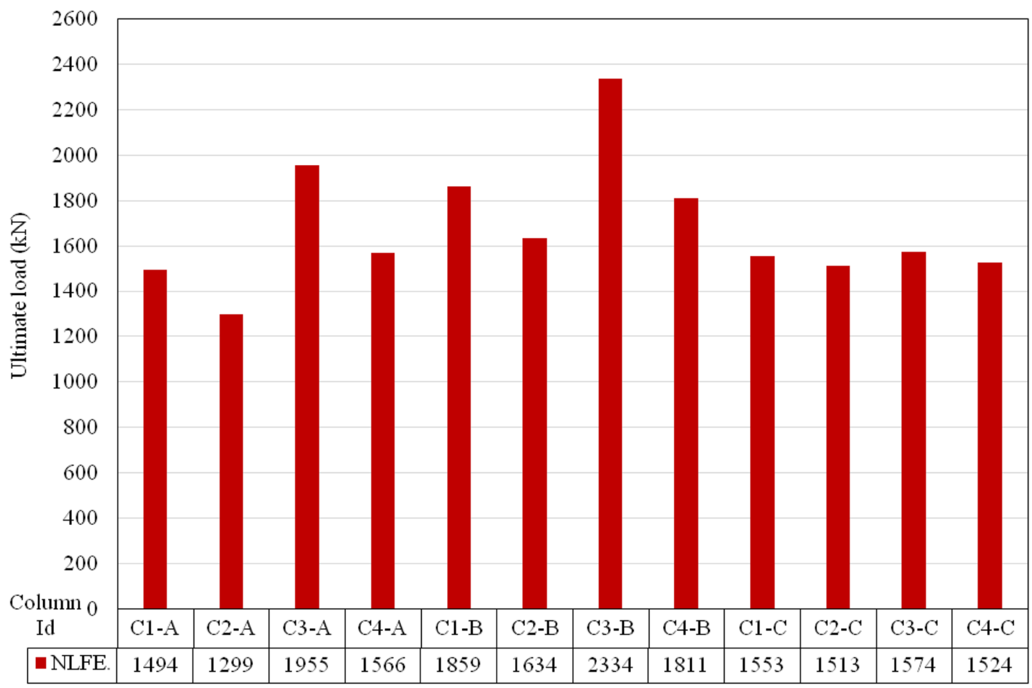

Fig. 11 Ultimate load for modeled columns

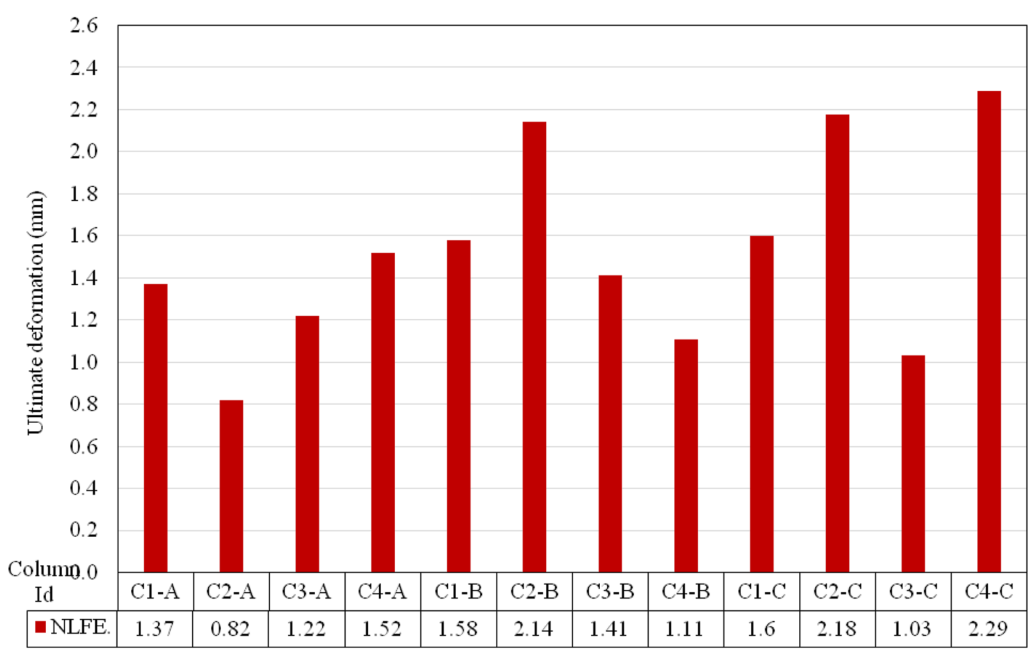

Fig. 12 Ultimate deflection for modeled columns

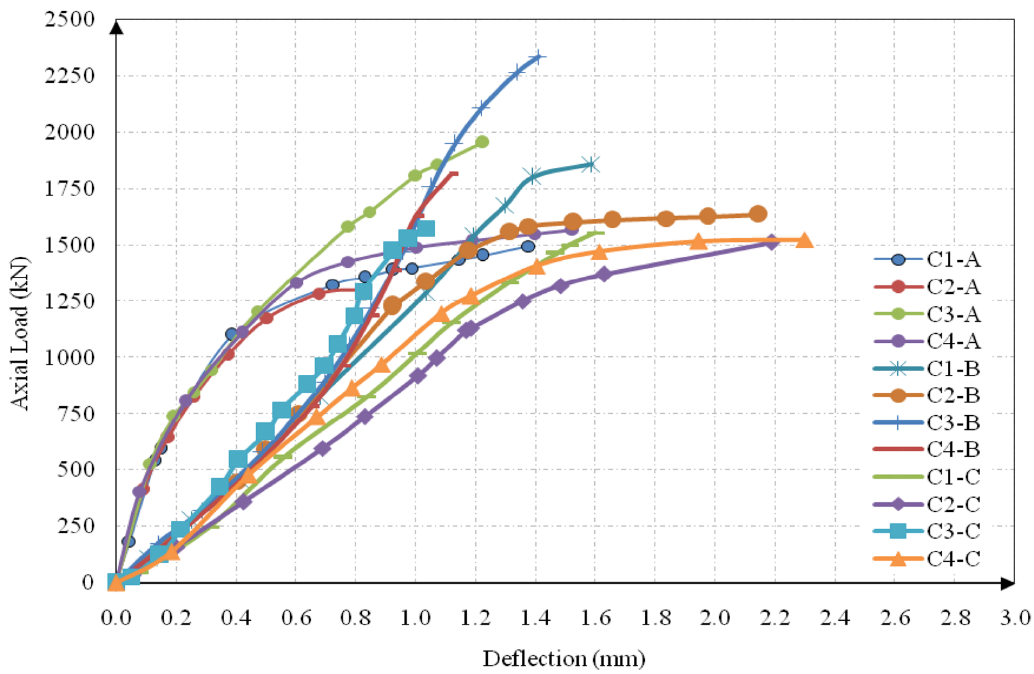

Fig. 13 Load–deflection curves for all modeled groups

- **Basalt rebars**

10. $E_s = 56$ kN/mm^2 (Ibrahim et al., 2015).
11. $f_y = 1400$ MPa (Ibrahim et al., 2015).
12. $\nu = 0.2$ (Ibrahim et al., 2015).
13. ϕ12 (As = 112 mm^2).

3.6 Modeling Results

3.6.1 Ultimate Load and Deformation

In this section, behavior of the modeled column specimens in terms of ultimate load and deflection, the relationship between load and deflection, and cracking patterns are presented (see Figs. 11, 12, 13, 14). In addition, Table 5 provides a summary of analytical results.

3.6.2 Cracking Pattern

The cracking patterns of each modeled column are shown in Fig. 14.

4 Results and Discussion

4.1 Axial Load Capacity of Columns

The experimental and analytical ultimate loads for all columns are presented in Table 6 and Fig. 15. Experimentally and analytically, the ultimate for group A ranged from 1412 to 2092 kN and 1299 to 1955 kN, respectively. The influence of confinement was demonstrated in column C3-A with stirrups 8@100, which recorded greater maximum force values than column C4-A with 8@150, with a 22.8% enhancement ratio. The ultimate for group B ranged from 1776 to 2537 kN empirically and theoretically, respectively. Furthermore, employing a greater longitudinal steel reinforcement ratio for group B columns than for group A columns resulted in higher failure pressures for group B columns compared to corresponding group A columns. While for group c, the ultimate ranges from 1640 to 1700 kN and 1513 kN to 1574 kN, respectively, empirically and theoretically. Basalt RC columns handle about 90% of the axial load as compared to steel RC columns. The analytical investigation using Ansys software aided in estimating the ultimate carrying capacity of UHPC columns.

Table 6 and Fig. 16 also indicate the discrepancy between the analytical and experimental deflections. The agreement between the modeled and experimental columns was satisfactory.

Figs. 17, 18, 19 show the load–deflection relationship for the tested columns. These data clearly show that the load and deflection for all columns can be divided into two zones, which are as follows: the first region is: the behavior was elastic up to the first signs of breaking, with a linear relationship between force and deformation. The transition from linearity to curviness marks the end of this cycle. As the test conditions varied, so did the range

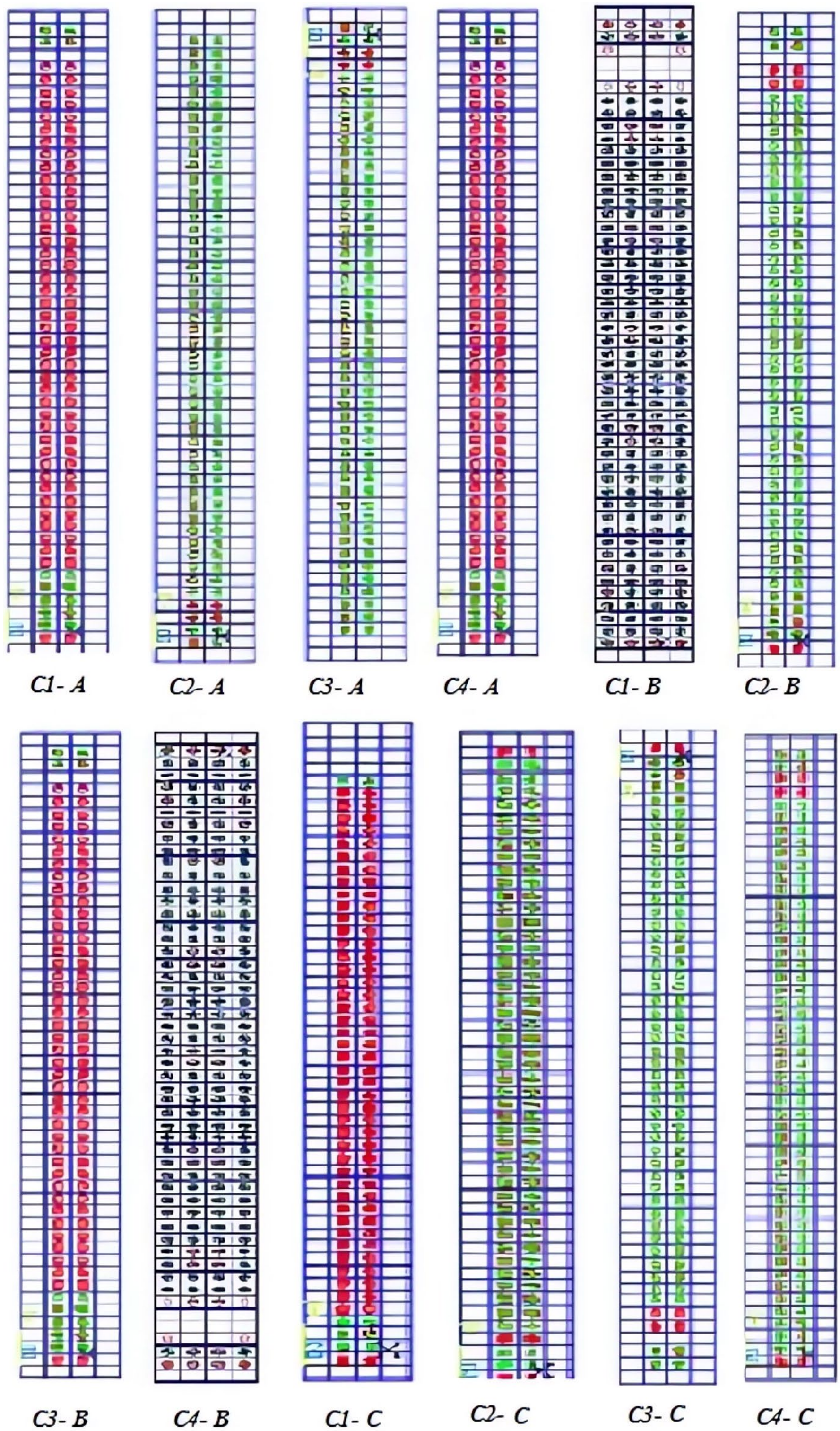

Fig. 14 Crack patterns for all modeled column

Table 5 Modeling results

Column ID	Ultimate load (kN)	Def. at Ult. load (mm)
C1-A	1494	1.37
C2-A	1299	0.82
C3-A	1955	1.22
C4-A	1566	1.52
C1-B	1859	1.58
C2-B	1634	2.14
C3-B	2334	1.41
C4-B	1811	1.11
C1-C	1553	1.60
C2-C	1513	2.18
C3-C	1574	1.03
C4-C	1524	2.29

of this stage. While in the second zone, the slope progressively changes as a result of the expected decrease in sample stiffness caused by serial cracking.

4.2 Mode of Failure

The first set of cracking was begun at the center of the column's length, as shown in Figs. 20, 21, and 22. This is due to the experiment's invisible micro-cracks. The experimental breaking force is somewhat less. This may be acceptable, because the FE analysis specifies the status of micro fractures. The fracture patterns at each load step, on the other hand, indicated that crack propagation for molded columns differed from the experimental one due to Ansys precision.

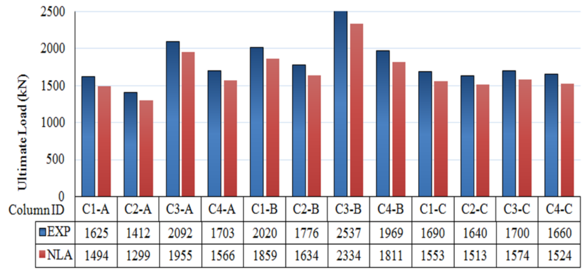

Fig. 15 Exp. and analytical ultimate load

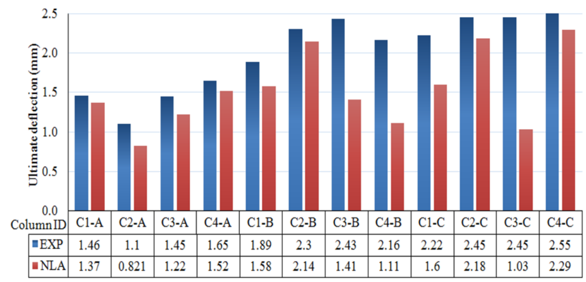

Fig. 16 Exp. and analytical ultimate deflection

4.2.1 Theoretical Study

The role of the basalt bars has not yet been identified by CSA (Afifi et al., 2014b) or ACI as no studies have been carried out (CSA, 2012). It was challenging to calculate the precise the ultimate loads of basalt-RC columns due to the many failure types.

As demonstrated in Eq. 1, Afifi et al. (ACI, 2015) were necessary for the CS of basalt bars. The compressive

Table 6 Results for experimental and analytical

Column ID	Ultimate load P_u (kN)		Def. at Ult. Load Δ_u (mm)		Pu_{NLA}/Pu_{EXP}	$\Delta_{u\,NLA}/\Delta_{u\,EXP}$
	NLA.	EXP.	NLA.	EXP.	–	–
C1-A	1494	1625	1.37	1.46	0.919	0.938
C2-A	1299	1412	0.82	1.10	0.920	0.746
C3-A	1955	2092	1.22	1.45	0.935	0.841
C4-A	1566	1703	1.52	1.65	0.920	0.921
C1-B	1859	2020	1.58	1.89	0.922	0.836
C2-B	1634	1776	2.14	2.30	0.925	0.930
C3-B	2334	2537	1.41	2.43	0.921	0.580
C4-B	1811	1969	1.11	2.16	0.920	0.514
C1-C	1553	1690	1.60	2.22	0.919	0.721
C2-C	1513	1640	2.18	2.45	0.923	0.890
C3-C	1574	1700	1.03	2.45	0.926	0.420
C4-C	1524	1660	2.29	2.55	0.918	0.898
Average					0.922	0.770
STD. dev.					0.005	0.180
Var.					0.00002	0.031

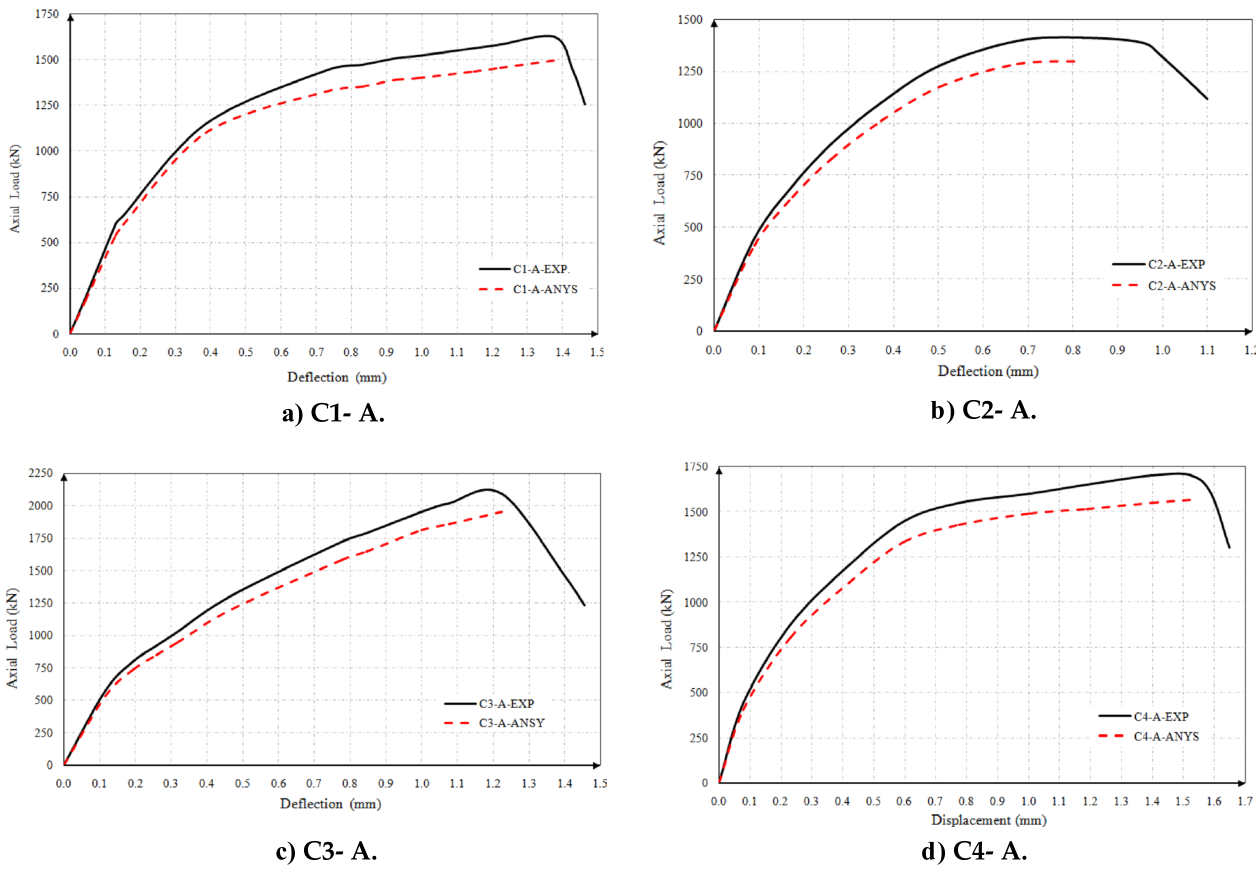

Fig. 17 Axial deformation response for group A

strength of basalt bars is estimated using Eq. 2 as per Tobbi et al. (Tobbi et al., 2012) linear-elastic theory. Although this model predicts a lesser strain level than the test, it yields a projected load that is lower than the exact load recorded in the research. According to Samani and Attard (Samani & Attard, 2012), the axial strain value for unconfined concrete cylinders is calculated by Eq. 3. According to the testing data, only the above three equations achieved axial loads of up to 60%, and Eq. 4 produced superior findings for both steel and basalt RC columns:

$$P_n = 0.85 \times f_c \times \left(A_g - A_{FRP}\right) + 0.35 \times f_{uFRP} \times A_{FRP} \quad (1)$$

$$P_n = 0.85 \times f_c \times \left(A_g - A_{FRP}\right) + 0.002 \times E_{FRP} \times A_{FRP} \quad (2)$$

$$P_n = 0.85 \times f_c \times \left(A_g - A_{FRP}\right) + 0.0025 \times E_{FRP} \times A_{FRP} \quad (3)$$

$$P_P = Ac\ Pck + As\ Psk \quad (4)$$

Table 7 shows the range of 60% between the estimated ultimate loads and those obtained experimentally using Eqs. 1, 2, 3. Equation 4 offered a satisfactory matching between axial capacity estimate findings depending on experimental results (IS456, 2000).

5 Conclusions

This research was conducted as an experimental and analytical investigation of the UHPC column with basalt bars under axial compression. The experimental and analytical results can be summarized as follows:

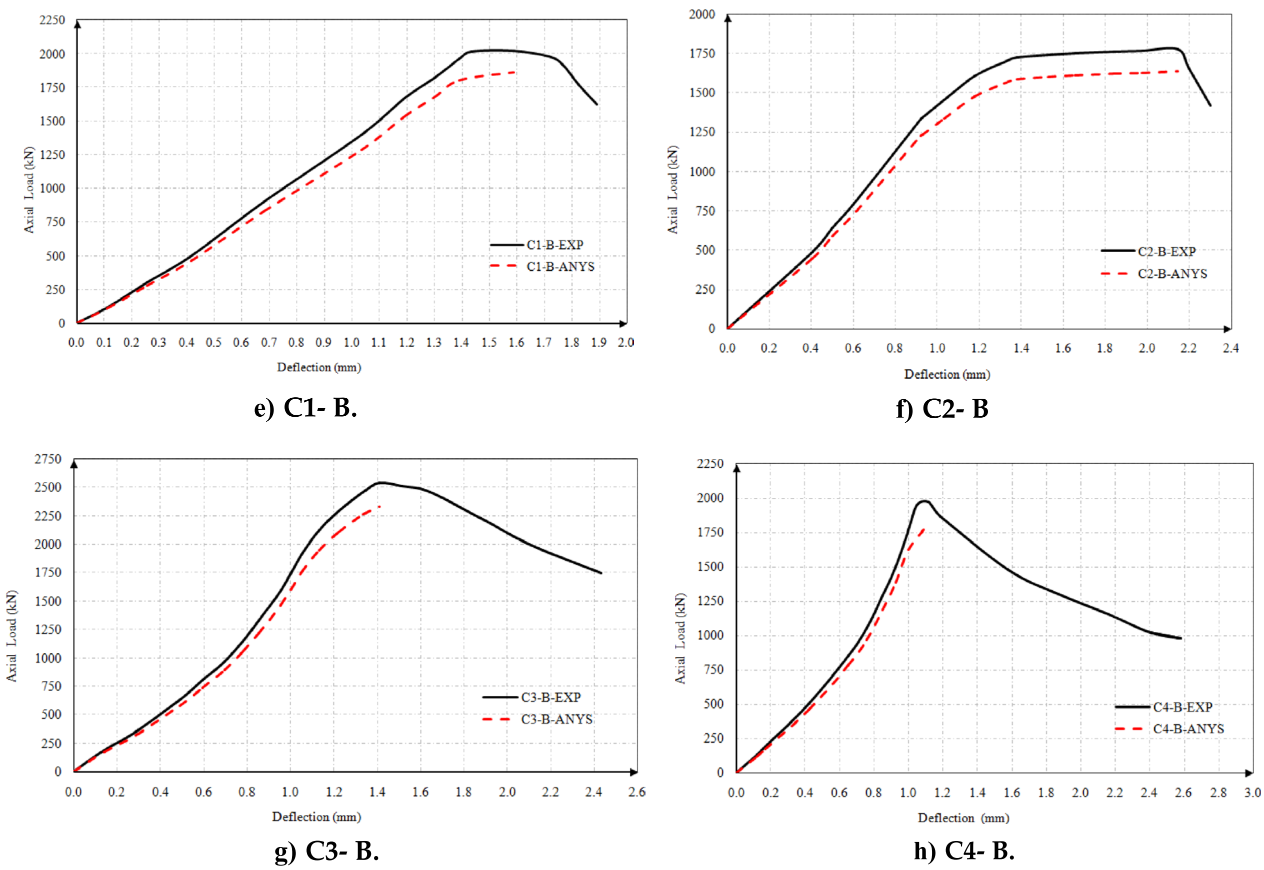

Fig. 18 Axial deformation response for group B

1- Increasing the highly longitudinal steel ratios for UHPC columns has an impact on the column carrying capacity; particularly when employing transverse reinforcement with tight spacing, which promotes confinement and raises carrying capacity.
2- In comparison with steel-reinforced UHPC columns, the basalt bars supported only around 90% of the axial load. According to the study, basalt bars might successfully replace steel reinforcement in circumstances, where corrosion is a danger.
3- The findings of the experiment and the analytical one show good agreement. The agreement is around 92.2%, with a standard deviation of 0.005 and a coefficient of variation of 0.00002.
4- When lateral deformation measurements for group C using basalt columns are contrasted with those for the other group using steel bars, the results reveal improved confinement, ductility, and energy absorption.
5- The created UHPC columns could be effectively employed as a replacement to the conventional RC columns, and in addition to its predicted economic and environmental benefits, may be beneficial in both developed and developing nations.
6- Equations are employed to forecast the strength of confined concrete. Eq. 4 merely produced improved forecasts, it aids in comparing the outcomes of analytical and experimental tests.

5.1 The Limitations and Future Research Direction of the Study

The following experimental research areas should be taken into consideration for subsequent investigation to enable a more thorough examination of the observed properties:

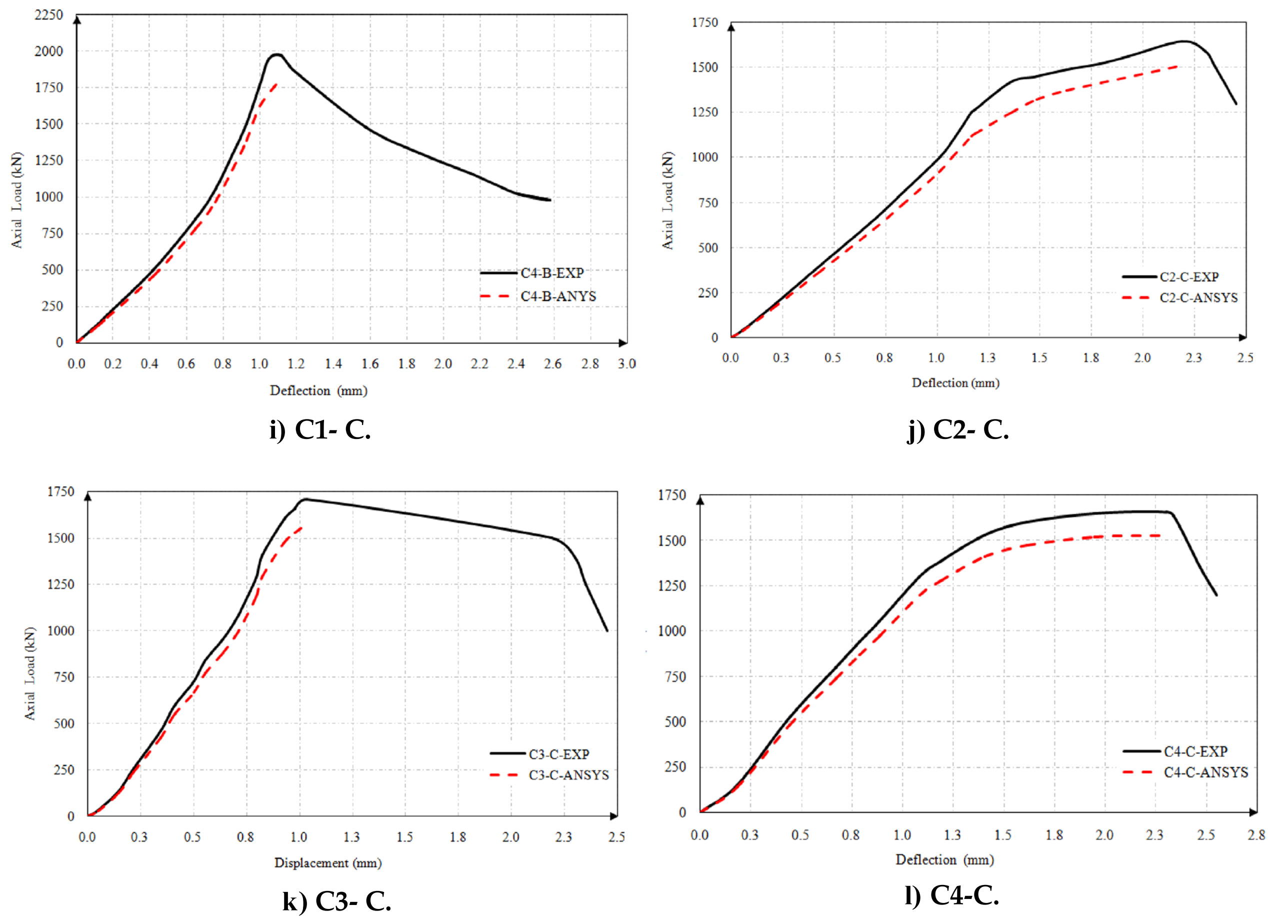

Fig. 19 Axial deformation response for group C

- Study the effect of confinement of steel stirrups with closely spaced less than 100 mm for BFRP longitudinal reinforcement for UHPC column under axial force.
- Using BFRP bars as longitudinal reinforcement with closely space transverse BFRP stirrups instead of steel stirrups for axial force UHPC columns.
- Effect of the eccentricity of force on UHP columns using BFRP bars instead of longitudinal steel bars.

Table 7 Comparison between test results and theatrical equations

Column ID	Experimental load (kN)	Equation (1) (kN)	Equation (2) (kN)	Equation (3) (kN)	Equation (4) (kN)
C1-A	1625	991.25	975.02	975.30	1755.00
C1-B	2020	1212.00	1191.80	1191.80	2161.40
C1-C	1690	929.50	946.40	929.50	1853.12

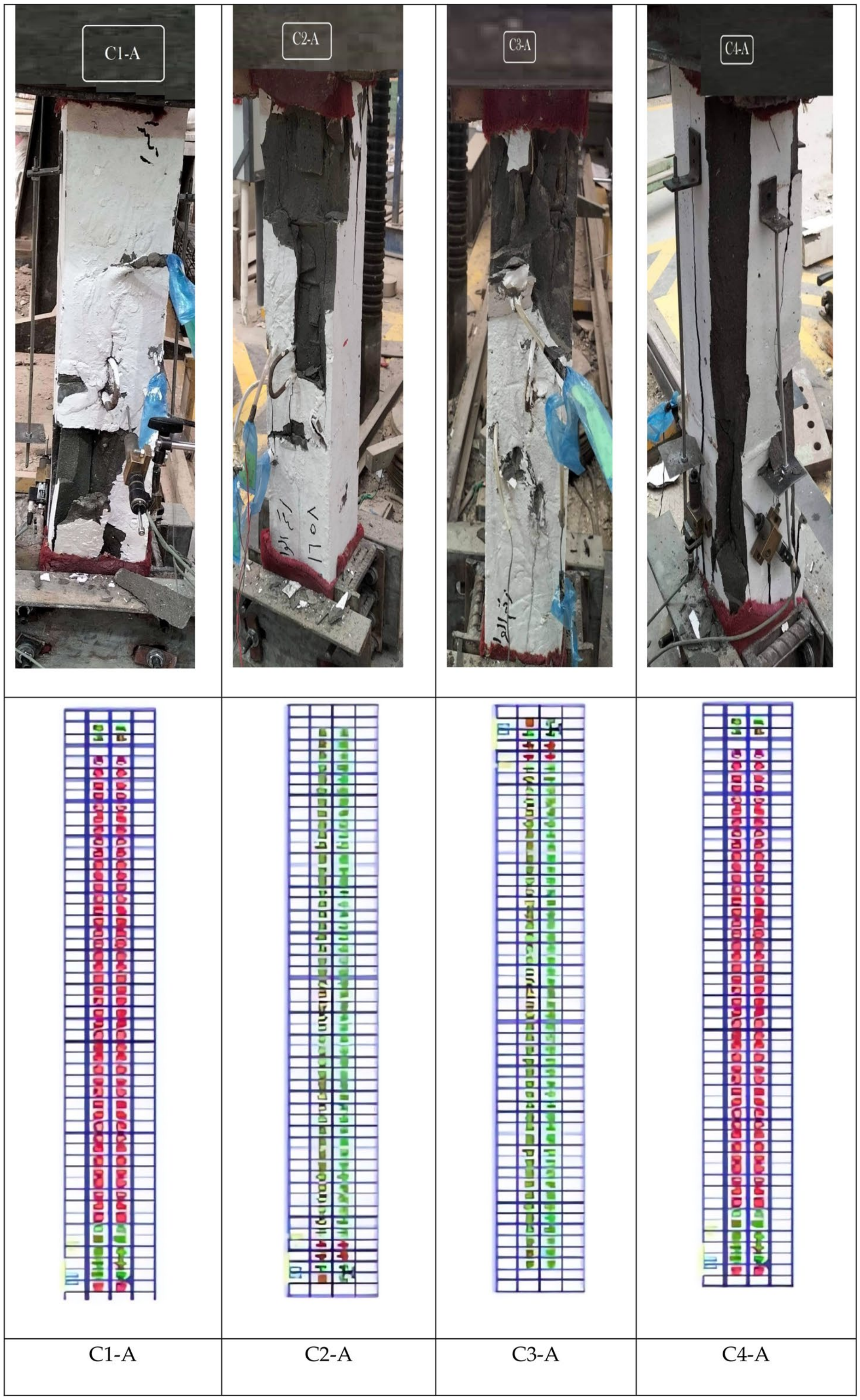

Fig. 20 Crack patterns for Group A

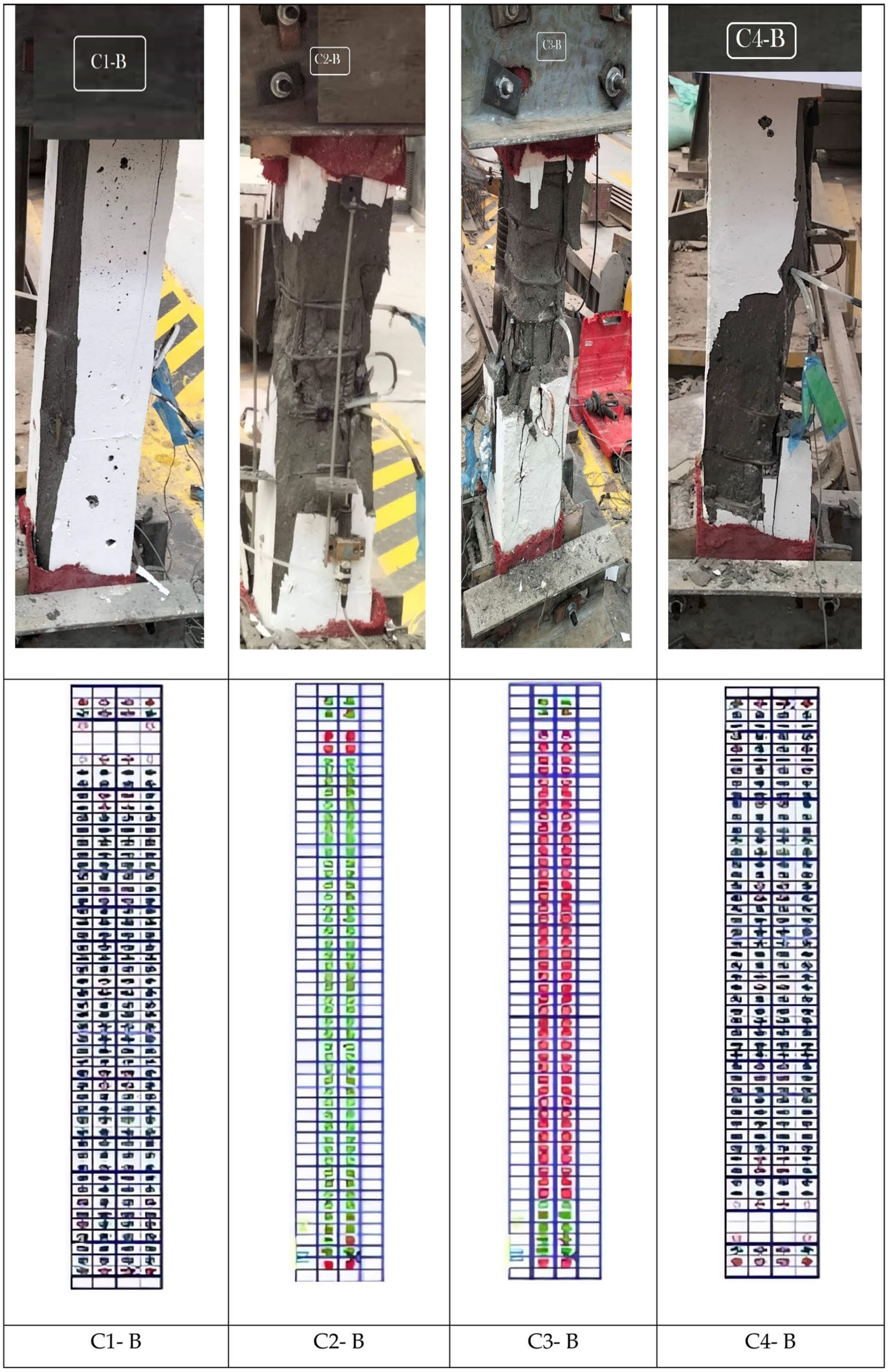

Fig. 21 Crack patterns for Group B

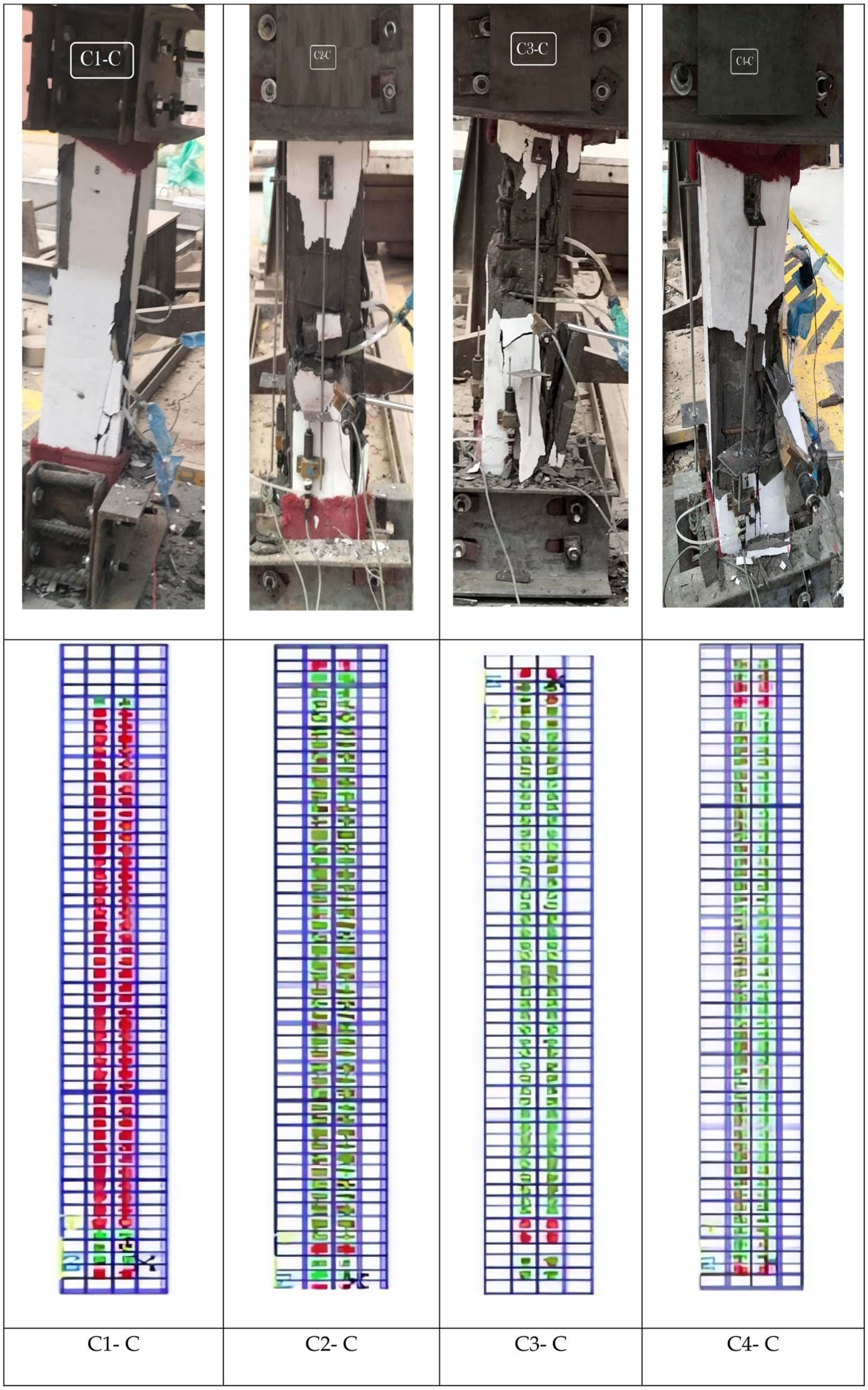

Fig. 22 Crack patterns for Group C

Acknowledgements
Not applicable

Author contributions
TAE-S: supervised the student, prepared the research plan, carried out the experimental work, shared in the theoretical work, and participated in writing and reviewing the article. KSG: wrote the article, carried out the experimental work, shared in the theoretical work and shared in the final revision. HHA: supervised the student, and revised the final revision. TA: supervised the student, and revised the final revision. All authors read and approved the final manuscript.

Author informations
Taha A. El-Sayed: BSc, MSc, PhD, Associate Professor, Associate Professor of Concrete Structures, Department of Structural Engineering, Shoubra Faculty of Engineering, Benha University, Cairo 11629, Egypt.
Kareem S. Abdallah: BSc, MSc, Teaching Assistant of Civil Engineering, Department of Structural Engineering, Shoubra Faculty of Engineering, Benha University, Cairo 11629, Egypt.
Hossam E. Ahmed: BSc, MSc, PhD, Professor of Civil Engineering, Department of Structural Engineering, Shoubra Faculty of Engineering, Benha University, Cairo 11629, Egypt.
Tamer H. El-Afandy: BSc, MSc, PhD, Professor of Civil Engineering, Housing and Building National Research Centre, Giza 12622, Egypt.

Funding
Open access funding provided by The Science, Technology & Innovation Funding Authority (STDF) in cooperation with The Egyptian Knowledge Bank (EKB).

Availability of data and materials
All data generated or analyzed during this study are included in this published article.

Declarations

Competing interests
The authors declare that they have no competing interests.

Received: 15 February 2023 Accepted: 29 March 2023
Published online: 07 August 2023

References

Abadel, A., Abbas, H., Almusallam, T., Alshaikh, I. M., Khawaji, M., Alghamdi, H., & Salah, A. A. (2022a). Experimental study of shear behavior of CFRP strengthened ultra-high-performance fiber-reinforced concrete deep beams. *Case Studies in Construction Materials, 16*, e01103.

Abadel, A. A., Abbas, H., Alshaikh, I. M., Tuladhar, R., Altheeb, A., & Alamri, M. (2023). March. Experimental study on the effects of external strengthening and elevated temperature on the shear behavior of ultra-high-performance fiber-reinforced concrete deep beams. *Structures, 49*, 943–957.

Abadel, A. A., Khan, M. I., & Masmoudi, R. (2022b). Experimental and numerical study of compressive behavior of axially loaded circular ultra-high-performance concrete-filled tube columns. *Case Studies in Construction Materials, 17*, e01376.

Abdellatief, M., AL-Tam, S. M., Elemam, W. E., Alanazi, H., Elgendy, G. M., & Tahwia, A. M. (2023). Development of ultra-high-performance concrete with low environmental impact integrated with metakaolin and industrial wastes. *Case Studies in Construction Materials, 18*, e01724.

ACI. (2015). Guide for the design and construction of concrete reinforced with FRP bars, (ACI), Farmington. Hills, Mich., USA

Adam, M. A., Erfan, A. M., Habib, F. A., & El-Sayed, T. A. (2021). Structural behavior of high-strength concrete slabs reinforced with GFRP bars. *Polymers, 13*(17), 2997.

Afifi, M. Z., Mohamed, H. M., & Benmokrane, B. (2014a). Strength and axial behavior of circular concrete columns reinforced with CFRP bars and spirals. *Journal of Composites for Construction, 18*(2), 04013035.

Afifi, M. Z., Mohamed, H. M., & Benmokrane, B. (2014b). Axial capacity of circular concrete columns reinforced with GFRP bars and spirals. *Journal of Composites for Construction, 18*, 04013017.

Al-Obaidi, S., Davolio, M., Monte, F. L., Costanzi, F., Luchini, M., Bamonte, P., & Ferrara, L. (2022). Structural validation of geothermal water basins constructed with durability enhanced ultra high performance fiber reinforced concrete (ultra high durability concrete). *Case Studies in Construction Materials, 17*, e01202.

American Concrete Institute (ACI). (2006). Guide for the design and construction of concrete reinforced with FRP bars. ACI 440.1R-06, Detroit

ANSYS. (2005) Engineering analysis system user's manual, and Theoretical Manual; Revision 8.0. Vol. 1, 2. Swanson Analysis System Inc.: Houston, PA, USA

ASTM D7205/D7205M-11. (2015) Standard test method for tensile properties of fiber reinforced polymer matrix composite bars. West Conshohocken, PA

Baby, F., Marchand, P., Atrach, M., & Toutlemonde, F. (2013). Analysis of flexure-shear behavior of UHPFRC beams based on stress field approach. *Engineering Structures, 56*, 194–206.

Baby, F., Marchand, P., & Toutlemonde, F. (2014). Shear behavior of ultrahigh performance fiber-reinforced concrete beams. I: Experimental investigation. *Journal of Structural Engineering, 140*(5), 04013111.

ISIS Canada. (2009). Intelligent sensing for innovative structures

Canadian Standards Association. (2012). Design and construction of building components with fiber reinforced polymers (CAN/CSA-S806-12). CSA Group, Mississauga, ON, Canada

Chaallal, O., & Benmokrane, B. (1993). Physical and mechanical performance of an innovative glass-fiber-reinforced plastic rod for concrete and grouted anchorages. *Canadian Journal of Civil Engineering, 20*(2), 254–268.

CSA. (2012). Design and construction of building structures with fibre-reinforced polymers

El Refai, A., Ammar, M. A., & Masmoudi, R. (2015). Bond performance of basalt fiber-reinforced polymer bars to concrete. *Journal of Composites for Construction, 19*(3), 04014050.

El-Sayed, T. A. (2021). Improving the performance of UHPC columns exposed to axial load and elevated temperature. *Case Studies in Construction Materials, 15*, e00748.

El-Sayed, T. A., & Algash, Y. A. (2021). Flexural behavior of ultra-high performance geopolymer RC beams reinforced with GFRP bars. *Case Studies in Construction Materials, 15*, e00604.

El-Sayed, T. A., Erfan, A. M., Abdelnaby, R. M., & Soliman, M. K. (2022). Flexural behavior of HSC beams reinforced by hybrid GFRP bars with steel wires. *Case Studies in Construction Materials, 16*, e01054.

EN 197-1:2011-Cement-Part 1: Composition, specifications, and conformity criteria for common cement

Erfan, A. M., Algashb, Y. A., & El-Sayed, T. A. (2019a). Experimental & analytical flexural behavior of concrete beams reinforced with basalt fiber reinforced polymers bars. *International Journal of Scientific and Engineering Research, 10*(8), 297–315.

Erfan, A. M., Algashb, Y. A., & El-Sayed, T. A. (2019b). Experimental and analytical behavior of HSC columns reinforced with basalt FRP bars. *International Journal of Scientific and Engineering Research, 10*(9), 240–260.

Erfan, A. M., Hassan, H. E., Hatab, K. M., & El-Sayed, T. A. (2020). The flexural behavior of nano concrete and high strength concrete using GFRP. *Construction and Building Materials, 247*, 118664.

Fang, C., Sadakkathulla, M. A., & Sheikh, A. (2019). Experimental and numerical study of ultra-high-performance fiber-reinforced concrete column subjected to axial and eccentric forces. *International Journal of Civil and Environmental Engineering, 13*(2), 79–85.

Ghareeb, K. S., Ahmed, H. E., El-Affandy, T. H., Deifalla, A. F., & El-Sayed, T. A. (2022). The novelty of using glass powder and lime powder for producing UHPSCC. *Buildings, 12*(5), 684.

Hosinieh, M. M., Aoude, H., Cook, W. D., & Mitchell, D. (2015). Behavior of ultra-high-performance fiber reinforced concrete columns under pure axial loading. *Engineering Structures, 99*, 388–401.

Hung, C. C., & Hu, F. Y. (2018). Behavior of high-strength concrete slender columns strengthened with steel fibers under concentric axial loading. *Construction and Building Materials, 175*, 422–433.

Ibrahim, A. M., Fahmy, M. F., & Wu, Z. (2015). Numerical simulation on fracturing bond mechanisms of different basalt FRP bars. 土木学会論文集 *A2 (*応用力学*), 71*(2), I_289-I_298.

IS 456. (2000). Plain concrete and reinforced, Indian standard. Delhi
Lachance, F., Charron, J. P., & Massicotte, B. (2016). Development of precast bridge slabs in high-performance fiber-reinforced concrete and ultra-high-performance fiber-reinforced concrete. *ACI Structural Journal, 113*(5), 929.
Lee, J. J., Song, J., & Kim, H. (2014). Chemical stability of basalt fiber in alkaline solution. *Fibers and Polymers, 15*(11), 2329–2334.
Li, W., & Xu, J. (2009). Mechanical properties of basalt fiber reinforced geopolymer concrete under impact loading. *Materials Science and Engineering: A, 505*(1–2), 178–186.
Liu, H., Lu, Z., & Peng, Z. (2015). Test research on prestressed beam of inorganic polymer concrete. *Materials and Structures, 48*(6), 1919–1930.
Mahmud, G. H., Yang, Z., & Hassan, A. M. (2013). Experimental and numerical studies of size effects of ultra high-performance steel fibre reinforced concrete (UHPFRC) beams. *Construction and Building Materials, 48*, 1027–1034.
Mallick, P. K. (1988). *Materials, manufacturing, and design*. New York: Marcell Dekker Inc.
Millard, S. G., Molyneaux, T. C. K., Barnett, S. J., & Gao, X. (2010). Dynamic enhancement of blast-resistant ultra-high-performance fibre-reinforced concrete under flexural and shear loading. *International Journal of Impact Engineering, 37*(4), 405–413.
Mohamed, H. M., Afifi, M. Z., & Benmokrane, B. (2014). Performance evaluation of concrete columns reinforced longitudinally with FRP bars and confined with FRP hoops and spirals under axial load. *Journal of Bridge Engineering, 19*(7), 04014020.
Nassif, M. K., Erfan, A. M., Fadel, O. T., & El-Sayed, T. A. (2021). Flexural behavior of high strength concrete deep beams reinforced with GFRP bars. *Case Studies in Construction Materials, 15*, e00613.
Ozbakkaloglu, T., Gholampour, A., & Xie, T. (2018). Mechanical and durability properties of recycled aggregate concrete: Effect of recycled aggregate properties and content. *Journal of Materials in Civil Engineering, 30*(2), 04017275.
Palacios, G. (2015). Performance of full-scale ultra-high-performance fiber-reinforced concrete column subjected to extreme earthquake-type loading and effect of surface preparation on the cohesion and friction factors of the AASHTO interface shear equation. The University OF Texas at Arlington.
Samani, A. K., & Attard, M. M. (2012). A stress-strain model for uniaxial and confined concrete under compression. *Engineering Structures, 41*, 335–349.
Shang, C., Wu, C., Wang, J., Lu, L., Fu, Q., Zhang, Y., & Song, X. (2022). Investigating mechanical properties and microstructure of reactive powder concrete blended with sulfoaluminate cement. *Case Studies in Construction Materials, 17*, e01552.
Shi, J. W., Zhu, H., Wu, Z. S., & Wu, G. (2011). Durability of BFRP and hybrid FRP sheets under freeze-thaw cycling. *Advances in Materials Research, 163*, 3297–3300.
Shin, H. O., Min, K. H., & Mitchell, D. (2017). Confinement of ultra-high-performance fiber reinforced concrete columns. *Composite Structures, 176*, 124–142.
Shin, H. O., Min, K. H., & Mitchell, D. (2018). Uniaxial behavior of circular ultra-high-performance fiber-reinforced concrete columns confined by spiral reinforcement. *Construction and Building Materials, 168*, 379–393.
Shin, H. O., Yoon, Y. S., Lee, S. H., Cook, W. D., & Mitchell, D. (2015). Effect of steel fibers on the performance of ultrahigh-strength concrete columns. *Journal of Materials in Civil Engineering, 27*(4), 04014142.
Tobbi, H., Farghaly, A. S., & Benmokrane, B. (2012). Concrete columns reinforced longitudinally and transversally with glass fiber-reinforced polymer bars. *ACI Structural Journal, 109*, 551–558.
Wang, Y., Jin, H., Demartino, C., Chen, W., & Yu, Y. (2022). Mechanical properties of SFRC: Database construction and model prediction. *Case Studies in Construction Materials, 17*, e01484.
Wei, B., Cao, H., & Song, S. (2010). RETRACTED: Environmental resistance and mechanical performance of basalt and glass fibers. *Materials Science and Engineering: A*. https://doi.org/10.1016/j.msea.2010.04.021
Wu, W. P. (1990). Thermomechanical properties of fiber reinforced plastic (FRP) Bars.) PhD Thesis. West Virginia University, Morgantown, West Virginia, USA
Xie, T., Fang, C., Ali, M. M., & Visintin, P. (2018a). Characterizations of autogenous and drying shrinkage of ultra-high-performance concrete (UHPC): An experimental study. *Cement and Concrete Composites, 91*, 156–173.
Xie, T., Fang, C., Ali, M. M., & Visintin, P. (2018b). Characterizations of autogenous and drying shrinkage of ultra-high performance concrete (UHPC): An experimental study. *Cement and Concrete Composites, 91*, 156–173.
Yoo, D. Y., Banthia, N., & Yoon, Y. S. (2015). Effectiveness of shrinkage-reducing admixture in reducing autogenous shrinkage stress of ultra-high-performance fiber-reinforced concrete. *Cement and Concrete Composites, 64*, 27–36.
Yu, Y., Yang, B. X., Liao, Z., Xu, J. J., Hu, S. W., & Zheng, Y. (2022). Uniaxial mechanical behaviors of recycled coarse aggregate concretes cast with conventional and equivalent mortar volume methods. *Advances in Structural Engineering, 25*(14), 2885–2905.
Yu, Y., Zheng, Y., & Zhao, X. Y. (2021). Mesoscale modeling of recycled aggregate concrete under uniaxial compression and tension using discrete element method. *Construction and Building Materials, 268*, 121116.
Zhu, Y., Zhang, Y., & Xu, Z. (2022). Analytical investigation of long-term behavior of normal concrete filled UHPC tube composite column. *Case Studies in Construction Materials, 17*, e01435.

Publisher's Note

Springer Nature remains neutral with regard to jurisdictional claims in published maps and institutional affiliations.